Archives of Virology (2019) 164:1069–1083
https://doi.org/10.1007/s00705-019-04175-3

ORIGINAL ARTICLE

Invasion of a murine *in vitro* blood-brain barrier co-culture model by dengue virus serotypes 1 to 4

Fakhriedzwan Idris[1,2] · Siti Hanna Muharram[2] · Zainun Zaini[3] · Sylvie Alonso[1] · Suwarni Diah[2]

Received: 28 March 2018 / Accepted: 16 January 2019 / Published online: 19 February 2019

Abstract

The blood-brain barrier (BBB) is a physical barrier that restricts the passage of cells and molecules as well as pathogens into the central nervous system (CNS). Some viruses enter the CNS by disrupting the BBB, while others can reach the CNS without altering the integrity of the BBB. Even though dengue virus (DENV) is not a distinctive neurotropic virus, the virus is considered to be one of the leading causes of neurological manifestations. In this study, we found that DENV is able to compromise the integrity of a murine *in vitro* blood-brain barrier (BBB) model, resulting in hyperpermeability, as shown by a significant increase in sucrose and albumin permeability. Infection of brain endothelial cells (ECs) was facilitated by the presence of glycans, in particular, mannose and N-acetyl glucosamine residues, on cell surfaces and viral envelope proteins, and the requirement for glycan moieties for cell infection was serotype-specific. Direct viral disruption of brain ECs was observed, leading to a significant decrease in tight-junction protein expression and peripheral localization, which contributed to the changes in BBB permeability. In conclusion, the hyperpermeability and breaching mechanism of BBB by DENV are primarily due to direct consequences of viral infection of ECs, as shown in this *in vitro* study.

Introduction

The blood-brain barrier (BBB) is a physical barrier that restricts the passage of cells and molecules as well as pathogens into the central nervous system (CNS) [1, 2], and hence, an increase in BBB permeability has frequently been linked to pathological changes in the CNS. Viruses that are known to be neurotropic have adopted a number of mechanisms by which they can invade the BBB and spread to the CNS paracellularly, transcellularly, and/or by hijacking circulating immune cells [3]. Some viruses, such as mouse adenovirus type 1 [4] and Nipah virus [5], enter the CNS by disrupting the BBB, while others can reach the CNS without altering the integrity of the BBB. Murray Valley encephalitis virus is thought to enter the CNS through the olfactory pathway, which is independent of BBB dysfunction [6]. West Nile virus (WNV) is believed to use multiple routes for entry into the CNS, although the mechanisms associated with CNS invasion have yet to be resolved [7]. These routes include retrograde axonal transport bypassing the peripheral nervous system, and through a 'Trojan horse' mechanism by infecting monocytes, dendritic cells, or macrophages [8]. In addition, an *in vitro* study has shown the ability of WNV to infect epithelial cells (ECs), suggesting that WNV might enter the BBB through brain ECs [9]. Likewise, the precise routes by which Japanese encephalitis virus (JEV) enters the CNS remain unclear. Entry of JEV into the CNS can occur via a haematogenous route, since complete diffusion has been observed throughout the brain during infection [10]. JEV is able to infect both macrophages and dendritic cells, which is suggestive of the 'Trojan horse' mechanism contributing to virus transmission into the CNS [11–13].

Even though dengue virus (DENV) is not a distinctive neurotropic virus, the virus is considered to be one of the

Handling Editor: Patricia Aguilar.

Electronic supplementary material The online version of this article (https://doi.org/10.1007/s00705-019-04175-3) contains supplementary material, which is available to authorized users.

✉ Fakhriedzwan Idris
micffhi@nus.edu.sg; fakhriedzwan.idris@gmail.com

[1] Department of Microbiology and Immunology, Yong Loo Lin School of Medicine, and Immunology Programme Life Sciences Institute, National University of Singapore, Singapore, Singapore

[2] Pengiran Anak Puteri Rashidah Sa'adatul Bolkiah Institute of Health Sciences, Universiti Brunei Darussalam, Jalan Tungku Link, Gadong BE1410, Brunei Darussalam

[3] Virology Laboratory, Clinical Laboratory Services, Ministry of Health, Gadong, Brunei Darussalam

leading causes of neurological manifestations [14, 15]. The mechanism by which DENV enters the brain during infection is unclear; several studies have suggested several mediators that may contribute to BBB breaching. Significant damage to the endothelium has been observed during infection, which can be mediated by cytokines, including IFN-γ [16] and TNF-α [17], by other biochemical molecules and apoptotic processes [18], and by possible cell destruction caused by cytotoxic events or the complement cascade. One or a combination of these events may modify the BBB and facilitate the passage of virus into the brain. A recent report described a fatal DENV4 case with the induction of rapid neurological deterioration starting at the onset of disease. The detection of large amounts of viral RNA in the cerebrospinal fluid in addition to the serum is suggestive of early entry of the virus into the CNS through the BBB, resulting in the observed neurological deterioration [19]. Alterations in BBB permeability were observed in adult mice after intracerebral inoculation with DENV2, and this was accompanied by the infiltration of immune cells and plasma proteins into the brain parenchyma, subsequently affecting neurological functions [20]. Similarly, an *in vivo* study in suckling mice showed that DENV infection of neurons and microglia was accompanied by BBB changes [21].

The neurovascular unit (NVU), which makes up the BBB, is composed of neurons as the main constituent in addition to brain microvascular ECs, pericytes, astrocytes, microglia, basal membrane and extracellular matrix. An earlier study has shown that astrocytes play a key role in the interactions and communications of neurons and brain ECs [22], which strengthens the finding that brain ECs, astrocytes, and neurons are the key elements of the NVU. Thus, on this basis, we have chosen these three cell types to develop a BBB model for the study of BBB breaching by DENV. The roles of microvascular endothelial cells and BBB modifications in the entry and spread of the virus associated with DENV infection have not been described. It is possible that the infection and subsequent changes to the BBB, especially the endothelial cells, promote the entry of DENV into nervous tissues, leading to brain infection and neuropathogenesis. Therefore, in the present study, we examined the ability of clinical isolates of DENV1-4 to infect brain cells and subsequently investigated the mechanism leading to BBB hyperpermeability during DENV infection using a newly developed *in vitro* triple co-culture BBB model.

Materials and methods

Virus and cells

Clinical isolates of DENV1 (GenBank accession no. MK069404), DENV2 (GenBank accession no. MK069405), DENV3 (GenBank accession no. MK034359), and DENV4 (GenBank accession no. MK034360) used in this study were obtained from Virology Laboratory, Clinical Laboratory Services, Ministry of Health, Brunei Darussalam. DENV isolates were propagated in Vero cells, harvested and stored at −80 °C in small aliquots, and used as the source of virus for all experiments.

Brain endothelial cells (bEnd.3, mouse BALB/c) CRL2299, astrocyte type III (C8-D30, mouse C57BL/6) CRL2534, neuroblastoma SH-SY5Y (human) CRL2266, and Vero CCL-81 (African green monkey) were purchased from American Type Culture Collection (ATCC). All cells except Vero cells were grown in DMEM (Sigma) containing 4500 mg of glucose L^{-1}, 110 mg of sodium pyruvate L^{-1} and sodium bicarbonate, supplemented with 10% fetal bovine serum (FBS), 2 mM L-glutamine and 100 I.U. of penicillin-streptomycin ml^{-1}. Vero cells were grown in MEM (ATCC) containing Earle's salts with 25 mM HEPES and sodium bicarbonate, supplemented with 10% FBS (Sigma), 2 mM L-glutamine (Sigma) and 100 I.U. of penicillin-streptomycin ml^{-1} (Sigma). One-half of the medium was changed every third or fourth day. The cell growth and viability were maintained under constant conditions of 37 °C, 5% CO_2 and a humidified atmosphere in a cell culture incubator.

Construction of *in vitro* triple co-culture BBB models

A triple culture system was established following the protocol described by Takata et al. [23] with modifications. The combination of cell lines was chosen as it had not been done previously and our results showed that this combination could cause bEnd.3 cells to acquire BBB characteristics as demonstrated by low permeability to sucrose and albumin (Supplementary Fig. 1). C8-D30 cells were seeded directly (5.0×10^4 cells ml^{-1}) on the basal side of Transwell inserts (polyester, 0.4 μm, Costar) and allowed to attach and proliferate on the insert for 2 days before being inverted. Inserts with confluent C8-D30 cells grown on the basal side were transferred to a well containing SH-SY5Y cells (5.0×10^4 cells ml^{-1}). bEnd.3 cells were then seeded (5.0×10^4 cells ml^{-1}) on the apical side, and the system was allowed to grow further until day 5 at 37 °C with a 5% CO_2 atmosphere.

Assessment of the permeability of the DENV-infected BBB model

The BBB model was infected with DENV 1-4 at a multiplicity of infection (MOI) of 5 for 6 or 24 hours. Transport assays using sucrose and albumin as paracellular and transcellular markers, respectively, were performed to assess the integrity of the infected model as described by Zhang et al. [24] with modifications. Briefly, inserts containing an endothelial cell monolayer were transferred to wells

containing phenol-red-free DMEM in the basal compartment. Then, 0.5 ml of the compounds (50 mg ml^{-1}) was added to the apical compartment, and the cells were incubated for 5, 10, 15, 20, and 30 minutes. One ml of medium was extracted from the basal compartment at each time point and measured using UV/VIS spectrometry (PerkinElmer Lambda 25) to determine the concentration of transported compounds. The concentration of each compound in the extracted samples was calculated based on the corresponding calibration curves. Subsequently, P_{app} values indicating the rates at which the compounds diffuse to the basal compartment of the Transwell were calculated using the following equation according to Hubatsch et al. [25]:

$$P_{app} = (dQ/dt)\left(1/\left(AC_0\right)\right),$$

where dQ/dt is the steady-state flux (µmol^{-1}), A is the surface area of the insert membrane (cm^2), and C_0 is the initial concentration in the donor chamber in µmol.

Western blot analysis

Cellular extracts were prepared in RIPA buffer containing 50 mM Tris, 150 mM NaCl, 1% NP40, 1 mM EDTA, 0.25% sodium deoxycholate, and 1% protease inhibitor cocktail (Sigma). The total protein concentration in the cell lysates was determined using a BCA protein assay (Pierce, Rockford, IL, USA). Equivalent amounts of protein from each sample were subjected to 10% SDS-PAGE followed by electrotransfer to a nitrocellulose membrane. The nitrocellulose membranes were blocked in TBS buffer containing 0.1% Tween 20 and 5% nonfat dry milk for 1 hour. Occludin, claudin-5, ZO-1, and GAPDH were detected using antibodies against occludin (1:2000, Abcam), claudin-5 (1:2000, Abcam), ZO-1 (1:500, Merck), and GAPDH (1:2000, Abcam) with overnight incubation at 4 °C, followed by incubation with HRP-conjugated anti-rabbit IgG antibodies. Clarity™ Western ECL substrate was used for protein detection, and imaging was performed using a Molecular Imager VersaDoc™ MP 4000 System (Bio-Rad). The relative intensity of the individual proteins was expressed relative to GAPDH and the total amount of protein.

Immunofluorescence assay

bEnd.3 cells on Transwell inserts were washed three times with phosphate-buffered saline (PBS) to remove medium before fixation in ice-cold acetone for 1 minute. Inserts were then washed twice with PBS to remove excess acetone. Two hundred µl of permeabilization buffer (0.2% Triton X-100, 2% bovine serum albumin [BSA]) was applied to each insert and incubated for at least 30 minutes. A third washing was done, and primary antibodies against DENV 1+2+3+4 (1:100, Abcam), occludin (1:1000, Abcam), claudin-5 (1:1000, Abcam), and ZO-1 (1:500, Merck) diluted in antibody signal enhancer (10 mM glycine, 0.05% Tween 20, 0.1% Triton X-100, 0.1% hydrogen peroxide in PBS) [26] were applied to each sample and incubated for 1 hour at room temperature. This was followed by incubation of the inserts with a conjugated secondary antibody (1:1000 dilution in permeabilization buffer) for 1 hour at room temperature. Subsequently, the inserts were washed three times with distilled water and mounted in glycerol/PBS (1:1). Imaging was done using a Nikon Eclipse 90i epifluorescence microscope equipped with a Nikon DS-Fi1 camera.

To quantify protein expression based on fluorescence intensity, a single in-focus plane was acquired according to McCloy et al. [27]. An outline was drawn around the fluorescent region of each cell, and the image was analyzed using Fiji/ImageJ software to obtain area and mean fluorescence measurements, as well as several adjacent background readings. The total corrected cellular fluorescence (TCCF) was calculated according to the formula below:

$$\text{TCCF} = \text{integrated density} - (\text{area of selected cell} \times \text{mean fluorescence of background readings}).$$

Binding assays

Binding assays were done as described by Alen et al. [28] with modifications. Two experimental conditions were used: a pre-binding assay and a pre-exposure assay. Cells were treated with lectins from *Galanthus nivalis* (*Galanthus nivalis* agglutinin [GNA]), *Lens culinaris* (*Lens culinaris* agglutinin [LCA]), *Datura stramonium* (*Datura stramonium* agglutinin [DSA]), and *Erythrina cristagalli* (*Erythrina cristagalli* agglutinin [ECA]) at concentrations of 200 and 400 µg ml^{-1} and from *Canavalia ensiformis* (concanavalin A[ConA]) at concentrations of 150 and 300 µg ml^{-1} based on the LC_{50} values (Supplementary Fig. 2). In the pre-binding assay, cells grown in 12-well plates were preincubated with lectins for 15 minutes at 4 °C, followed by incubation with DENV (MOI of 5) for 15 minutes at 4 °C, a temperature that allows virus binding to occur, but not virus internalization into the cells. Cells were washed extensively, with PBS after the incubation period to remove unbound virus and then further incubated for two days before analysis. In the pre-exposure assay, DENV was preincubated in the lectin suspension for 30 minutes at 4 °C. The mixtures were then applied to the cells, which were incubated for 4 hours at 37 °C with 5% CO_2. The cells were then washed thoroughly and incubated for another two days before analysis.

Flow cytometry

Treated cells were detached from plates and fixed in 4% paraformaldehyde at 4 °C for 15 minutes and permeabilized with cytofix/cytoperm buffer. They were then pelleted

at 1500 rpm for 3 minutes, followed by incubation with the anti-dengue 1+2+3+4 antibody (1:100, Abcam), and subsequently with an Alexa Fluor 488–conjugated secondary antibody (1:1000, Cell Signaling Technology). Incubation with antibodies was performed at 4 °C for 30 minutes. The stained cells were washed thoroughly and filtered through a 50-µm nylon mesh before being analyzed using a BD Accuri C6 flow cytometer.

Migration assay

The BBB model was infected with DENV 1-4 at an MOI of 5 and incubated at 37 °C with 5% CO_2. Medium was collected from the upper and lower chamber every 6 hours up to 24 hours, and virus particles were quantitated using a $TCID_{50}$ assay.

$TCID_{50}$ assay

The purpose of the assay was to determine the dilution of virus required to infect 50% of a given batch of inoculated cell cultures. The protocol was adapted and modified from Malenovska [29]. Vero cells were seeded in a 96-well plate (Corning CELLBIND^{TM}) at a seeding concentration of 5.0 $\times 10^4$ cells ml^{-1}. Tenfold serial dilutions of virus suspension of each serotype were prepared in maintenance medium. The growth medium was removed, and 100 µl of each virus dilution was added to the wells in six replicates. Plates were incubated at 37 °C in a 5% CO_2 atmosphere. The development of a cytopathic effect (CPE) was examined in each well at day 4 postinfection and recorded. The $TCID_{50}$ was calculated using Reed-Muench method and formula.

Statistical analysis

All results were expressed as the mean ± SD from three or more independent experiments. Statistical significance was assessed by 2-way ANOVA multiple comparison tests. A *p*-value less than 0.05 was considered significant. All statistical analysis was performed using GraphPad Prism 7.0 for Windows (GraphPad Software, San Diego, California, USA).

Results

Cell tropism of DENV

To establish an infection, DENV should be able to attach to and invade the cells used in this study. Therefore, a series of infection experiments was done to determine the susceptibility of brain endothelial cells (bEnd.3), astrocytes (C8-D30), and neuron cells (SH-SY5Y) to DENV. Cell death due to DENV infection was confirmed by the presence of fragmented bright blue nuclei (white arrows) when staining with 4′,6-diamidino-2-phenylindole (DAPI), indicating chromatin condensation, surrounded by an apoptotic body of infected cells and shrunken cytoplasm [30]. As shown in Fig. 1, all serotypes readily infected all three types of brain cells when inoculated at an MOI of 5 for 4 hours. Virus localization (yellow arrows) was seen in the cytoplasm of infected cells in which signs of death were observed, with shrinking and contraction of the cytoplasm. SH-SY5Y appeared elongated, with a gradual loss of neurites, and the appearance of cell clumps was observed. Morphological observation of infected astrocytes showed typical CPE, including swelling, rounding, and enhanced refraction, unlike uninfected astrocytes, which exhibited polygonal, flattened morphology.

Roles of mannose- and N-acetyl glucosamine (GlcNAc)-rich glycans in the infection of brain ECs by DENV

We further characterized the carbohydrate-bearing receptors targeted by DENV during infection of bEnd.3 cells using a pre-binding assay. In this assay, cells were preincubated with each lectin for 15 minutes at 4 °C, followed by incubation with DENV1-4 at an MOI of 5 for 15 minutes at 4 °C. bEnd.3 cells were washed to remove unbound virus, and infected cells were incubated for two days before analysis. Mannose- and N-acetyl-glucosamine-specific lectins showed variations in their inhibition patterns when cells were preincubated with lectins prior to infection (Fig. 2). It was observed that only ConA showed relatively high inhibition against all serotypes, with the highest recorded value being 55.7 ± 4.4% for DENV1. This was followed by LCA which showed significant dose-dependent inhibition of serotypes 1 (57.8 ± 9.4%), 2 (31.4 ± 3.6%) and 4 (29.7 ± 3.4%), but low inhibition against serotype 3, which was below 10%. GNA exhibited the highest inhibition when tested against DENV3 (33.8 ± 5.0%). Similar patterns of inhibition were observed for GlcNAc-specific lectins when tested against DENV2, 3 and 4. There was no significant inhibition observed when DSA was tested against DENV1, indicating that this serotype does not target the carbohydrate residue on bEnd.3 cells during infection.

The results indicated that DENV1, 2 and 4 prefer terminal mannosyl (LCA) and α-linked mannosyl-bearing (ConA) receptors, while DENV3 targets high-mannose (GNA)-rich receptors on bEnd.3 cells for infection. The results further showed that a combination of sialylated (ECA) and repeating units (DSA) of GlcNAc-bearing receptors are targeted by DENV2, 3 and 4. However, the presence of these GlcNAc residues was not a prerequisite for a successful infection of bEnd.3 cells by DENV1.

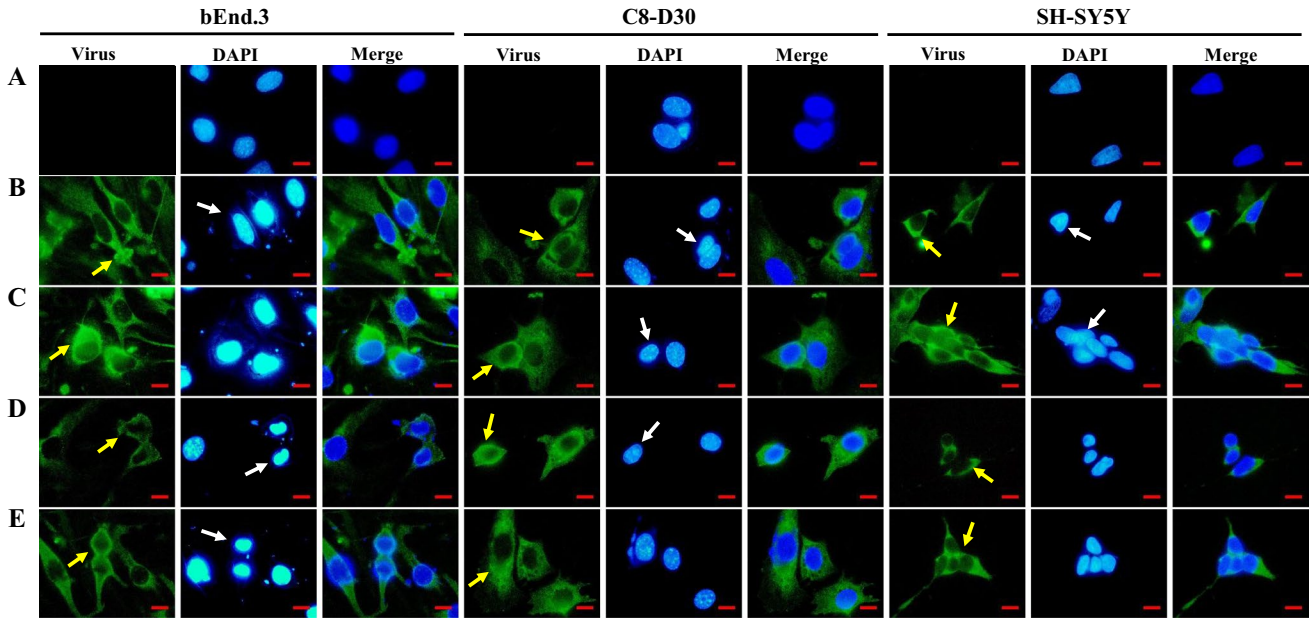

Fig. 1 DENV infection of bEnd.3, C8-D30 and SH-SY5Y cells at 4 hours postinfection. The virus was inoculated at an MOI of 5. A) Control (uninfected bEnd.3 cell monolayer), B) infection with DENV1, C) infection with DENV2, D) infection with DENV3, E) infection with DENV4. DENV was detected using DENV 1+2+3+4 antibody (Abcam) and was counterstained with Alexa Fluor 488 (Abcam). Scale = 50 µm

Glycan profiling of the E glycoprotein was performed using a pre-exposure assay in which DENV was pre-incubated with lectins in a suspension at 4 °C before being introduced onto the bEnd.3 monolayer. Similar to the pre-binding assay, variations in the inhibition patterns were also observed with mannose- and GlcNAc-specific lectins (Fig. 3). A strong dose-dependent inhibition was seen with ConA against DENV 1, 2 and 4, with the maximum value (54.7 ± 1.6%) obtained with DENV4, but only a moderate inhibitory effect was observed with DENV3. Although LCA showed the same pattern of inhibition against the other DENV serotypes (50.3 ± 3.7% with DENV1, 38.2 ± 4.0% with DENV3 and 17.2 ± 1.4% with DENV2), significant inhibition of DENV4 was only observed when the dose of LCA was increased to 400 µg ml^{-1} (19.6 ± 2.1%). On the other hand, the high-mannose-binding lectin GNA exerted less effect on all serotypes compared to ConA and LCA, with minimal or no inhibition of DENV2 and 1. DSA was demonstrated to be highly inhibitory against serotypes 2, 3 and 4, with a maximum of 57.1 ± 1.4% with DENV2, but not DENV1 with which the inhibition was below 15%. High inhibitory effects were only seen against DENV1 and 3 when challenged with ECA lectin, and inhibition was only observed for DENV4 when the lectin concentration was increased to 400 µg ml^{-1}.

The glycan profiles show that the presence of terminal-mannose (ConA and LCA) on the DENV envelope protein of all serotypes is essential for infection. To some degree, only DENV3 and 4 required high-mannose (GNA)-rich glycans on the E proteins for infection. Furthermore, DENV1 and 3 required sialylated GlcNAc (ECA) rather than repeating units of GlcNAc (DSA), but the opposite was observed for DENV2 and 4.

In vitro BBB hyper-permeability during infection

We then investigated whether infection leads to changes in the permeability of the BBB *in vitro* by infecting the triple co-culture model and measuring the paracellular and transcellular integrity of the infected model. For this purpose, we measured the amount of sucrose or albumin present in the supernatant of the lower chamber every 5 minutes up to 30 minutes after 6 and 24 hours of infection with DENV. Figure 4 shows the permeability data for sucrose and albumin during DENV infection of the BBB model. None of the controls showed changes in the permeability of sucrose or albumin. During infection, all serotypes caused a significant increase in sucrose influx across the triple co-culture model 6 hours postinfection, with an average increase of 20.2-fold. A further increase in the influx was also observed when the infection period was prolonged to 24 hours, with a 76.5-fold increase seen when the cells were infected with DENV4.

The results for albumin permeability in the infected BBB model showed a trend similar to that of sucrose, in which up to a 35.8-fold increase was observed 6 hours postinfection. The influx further increased significantly after 24 hours, in

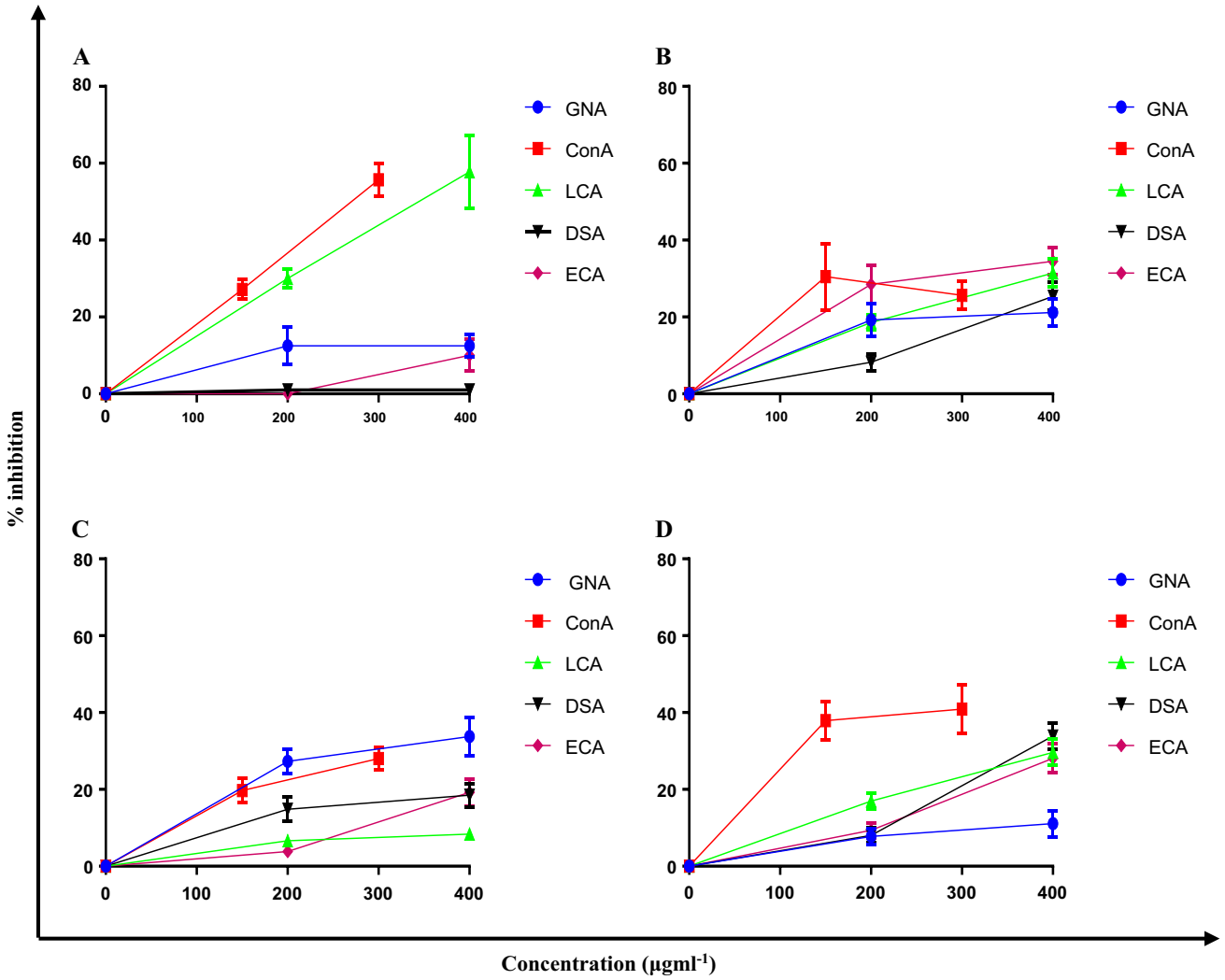

Fig. 2 Characterization of mannose- and N-acetyl-glucosamine-bearing receptors on bEnd.3 cells targeted by DENV. A) DENV1, B) DENV2, C) DENV3, D) DENV4. Data represent the mean ± SD from three independent experiments (n = 6)

the range between 59.4- and 74.8-fold, with all serotypes. Due to the compromised paracellular route, as shown by the increase sucrose permeability, albumin was able to cross paracellularly as well as transcellularly, which might explain the excessive influx of albumin seen in this study. These observations suggest that DENV breaches the BBB mainly through the paracellular route, damaging the structure in the process.

Alterations of TJ protein expression and localization in DENV-infected ECs

The integrity of the BBB is dictated by expression of TJ proteins and their distribution in brain ECs. Localization or redistribution of TJ proteins from tight junctions can also result in loss of BBB integrity. Hence, we detected and quantified TJ proteins, including occludin, claudin-5, and ZO-1, in bEnd.3 cells using the Western blot technique to investigate possible alterations in TJ protein expression during DENV infection. Protein expression was compared at 6 hours postinfection, which is early in the infection, and 24 hours postinfection, which is late in the infection. Western blot analysis showed different patterns of alteration in TJ protein expression. The data shown in Fig. 5B and C indicate that DENV infection did not decrease the levels of occludin or claudin-5. Instead, the expression levels of both TJ proteins, but particularly claudin-5, were significantly increased as a result of DENV infection. For example, at 6 hours postinfection, claudin-5 expression levels were 1.3- to 1.9-fold higher than in control samples, but they returned to normal when the infection period was extended to 24 hours. There was an exception for DENV2-infected bEnd.3 cells, in which a further significant 2.7-fold increase was observed. On the other hand, ZO-1 expression levels (Fig. 5D) steadily

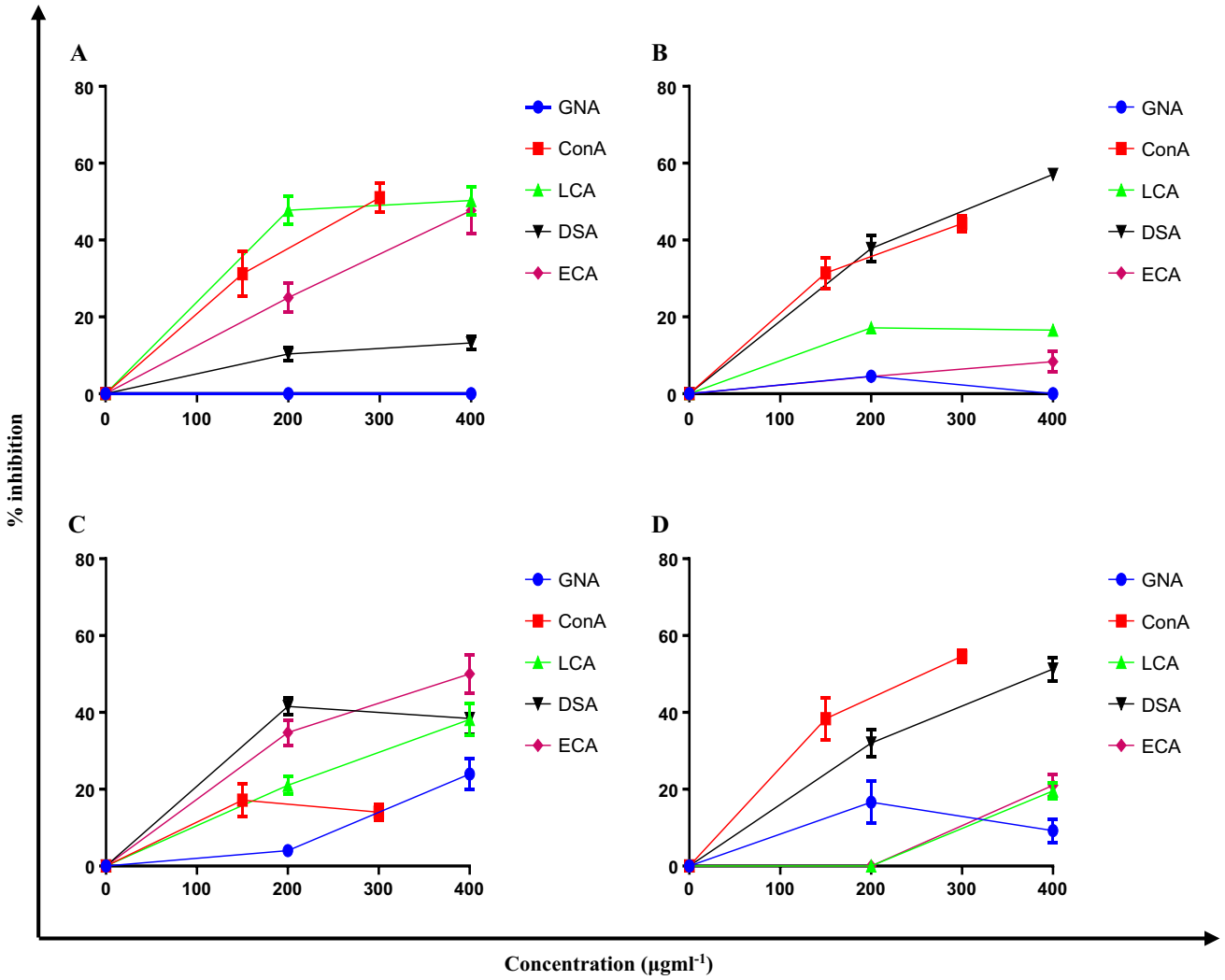

Fig. 3 Profiling of mannose- and N-acetyl-glucosamine on the DENV envelope protein essential for infection. A) DENV1, B) DENV2, C) DENV3, and D) DENV4. Data represent the mean ± SD from three independent experiments (n = 6)

decreased with prolonged infection time and were 1.3- to 4.4-fold lower than the control at 24 hours postinfection.

Since the expression levels of TJ proteins other than ZO-1 were relatively constant during infection, we assessed the distribution and staining pattern of these TJ proteins in infected cells by immunofluorescence assay as shown in Fig. 6. Occludin is normally localized at the periphery, as demonstrated by bright continuous lines in control cells, and is responsible for the restrictive properties of the BBB. However, when bEnd.3 cells were infected with DENV, occludin was found to be completely lacking from the periphery as early as 6 hours postinfection and had possibly diffused and relocated in the cytoplasm, as indicated by an increase in cytoplasmic fluorescence intensity. Similar patterns were observed in all cells infected with the different serotypes.

The peripheral localization and distribution of claudin-5 and ZO-1, on the other hand, were relatively unchanged. Infection of bEnd.3 cells for 6 hours did not significantly affect the fluorescence intensity of claudin-5. However, at 24 hours postinfection, claudin-5, which was generally localized along the contour of the TJ at the cell periphery in a continuous line, became discontinuous (yellow arrows), and claudin-5 aggregates appeared in the cytoplasm, with up to 96.5% reduction observed with DENV4 (Fig. 6E). The distribution of ZO-1 was affected as early as 6 hours postinfection, and apparent fragmentation of the protein was observed at locations where cell-cell contact occurred. The staining intensity of ZO-1 at the periphery also gradually decreased and became disarrayed (yellow arrows), with an increase in cytoplasmic diffusion, particularly around the nucleus during prolonged infection. Subsequent analysis of peripheral intensity revealed a significant reduction in ZO-1 during infection with all serotypes (up to 52.8% at 6 hours postinfection and up to 85.8% at 24 hours postinfection)

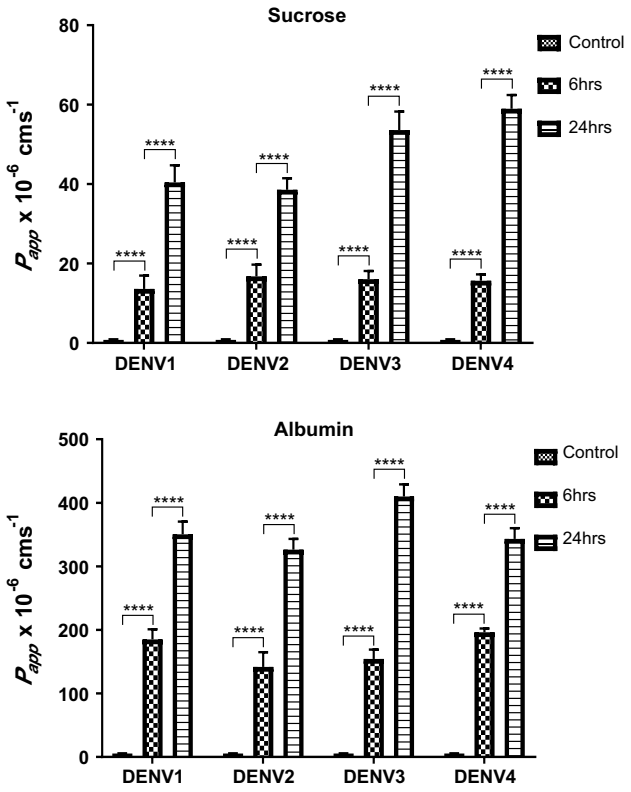

Fig. 4 Assessment of the permeability of the triple co-culture model when challenged with DENV. The BBB model was inoculated with virus at an MOI of 5 and incubated for 6 or 24 hours. The permeability of the infected model was assessed by measuring the transport of sucrose and albumin. Asterisks indicate significance (****, $p < 0.0001$)

(Fig. 6F). Protein aggregates and increased fluorescence in the cytoplasm may indicate that the protein was being removed from the cell membrane. These alterations were temporally associated with the gradual increase in permeability caused by virus infection.

Migration and paracellular transport of DENV

To date, there have been few studies examining the ability of DENV to infect and replicate in cells of the BBB, particularly ECs. Therefore, we investigated the replication kinetics in bEnd.3 cells by quantitating DENV in the supernatant from the upper chamber, collected every 6 hours up to 24 hours after infection, using a $TCID_{50}$ assay as shown in Fig. 7. There were variations in the infection period between DENV serotypes, with productive replication indicated by release of virions. No significant increase was observed in DENV2, 3 and 4 titers between 0 to 12 hours postinfection. However, the DENV1 titer increased significantly as early as 6 hours after the initial inoculation. Viral titers continued to increase significantly for all serotypes and peaked at 24 hours after infection, with titers ranging between 10.1 ± 1.3 and 11.8 ± 1.9 log $TCID_{50}$ ml^{-1}. In parallel, DENV-infected cells were also examined for CPE by phase contrast microscopy to confirm the infection and correlate it with the increased replication of the virus in bEnd.3 cells.

We also determined the ability of cell-free DENV to migrate across the BBB model by quantitating DENV present in the supernatant of the lower chamber. The viability of DENV released in the lower chamber, collected at various time points, was determined by $TCID_{50}$ assay (Fig. 7). Infectious virus was detected only after 12 hours postinfection, except in the case of DENV3, which was first detected at 6 hours postinfection, although the amount was not significant. DENV gradually migrated across the bEnd.3 monolayers as the infection period was extended in parallel to the increase in viral replication in the upper chamber. The migrated DENV peaked at 24 hours postinfection, with the highest titer (5.2 ± 0.7 log $TCID_{50}$ $ml^{-1)}$ obtained with DENV4. There was no significant migration of DENV3 observed across the culture model, even though there was an increasing trend during the infection period.

Discussion

Severe dengue virus infections in some cases lead to neurological symptoms. Although the neuropathogenesis of DENV has been investigated, the mechanism by which it occurs is not fully understood. In this study, we examined the ability of clinical isolates of DENV1-4 to infect brain cells and subsequently investigated the mechanism leading to BBB hyper-permeability during DENV infection using an *in vitro* triple co-culture BBB model.

We first investigated the ability of DENV isolates to infect the brain cell types used in this study. Previous studies have reported the detection of DENV antigens in various brain cells, including endothelial and perivascular cells, astrocytes, neurons, and microglia or the detection of viral RNA by RT-PCR in brain tissue samples [31–33]. In the current study, we found that bEnd.3 cells were prone to infection with all serotypes of DENV. Modification of the endothelium due to infection has been described in fatal cases of severe dengue [16, 34]. A study by Avirutnan et al. [35] demonstrated the susceptibility of human umbilical vein endothelial cells (HUVECs) to DENV2, and the infection resulted in the secretion of immune mediators that are involved in changes in vascular permeability, suggesting that viral infection of the endothelium contributes to dengue pathogenesis by increasing viremia and levels of inflammatory molecules as well as by making the endothelium a target for the cellular and humoral immune response. On the other hand, DENV-infected ECs in different organs, including the brain of a murine model, have been associated with

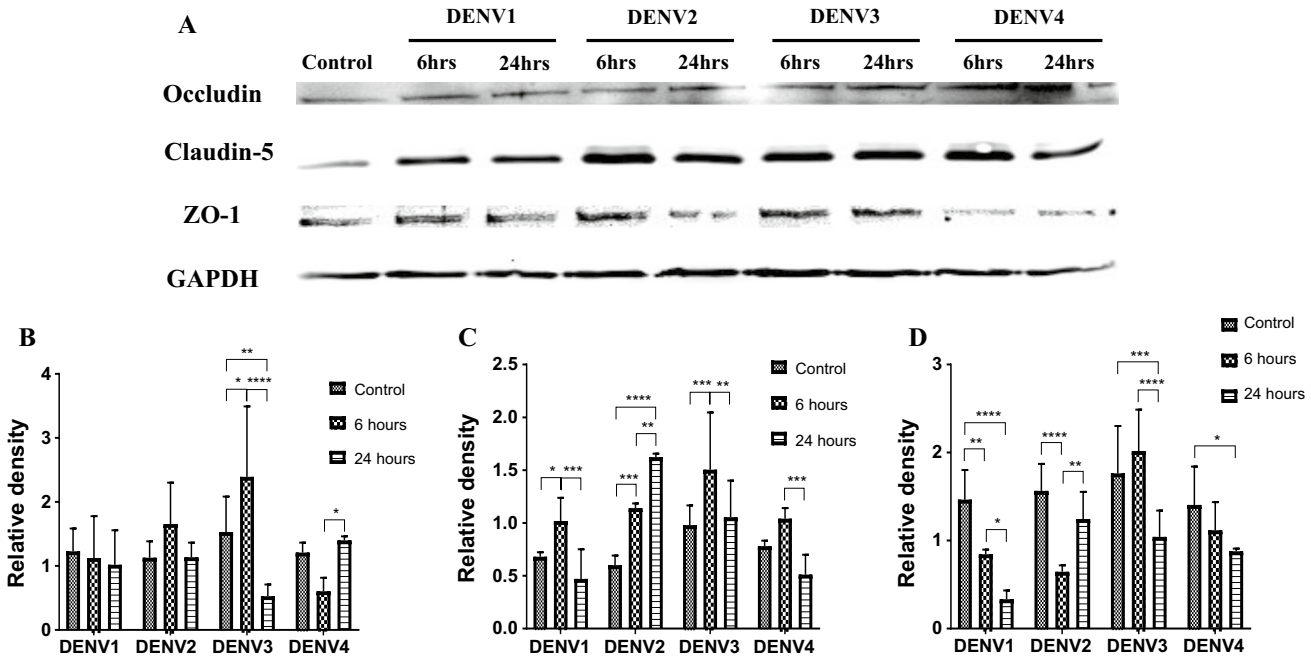

Fig. 5 Expression of TJ proteins in bEnd.3 cells challenged with DENV as determined by Western blotting. A) Protein expression was detected in DENV-infected bEnd.3 cell extracts 6 and 24 hours post-treatment. The relative densities of B) occludin, C) claudin-5, and D) ZO-1 bands were quantified using ImageJ software with GAPDH as a reference. Data are presented as the mean ± SD from three independent experiments ($n = 6$). Asterisks indicate significance (*, $p < 0.05$; **, $p < 0.01$; ***, $p < 0.001$; **** $p < 0.0001$)

increased production of TNF-α, bleeding, and eventually endothelial dysfunction [36, 37].

Interestingly, conflicting observations regarding the susceptibility of astrocytes to DENV infection have been reported. In studies by Velandia-Romero et al. [38] and Imbert et al. [39], astrocytes were reported to be resistant to DENV infection, while in our study, these cells were susceptible to all DENV serotypes. These discrepancies may be due to the genetic variations in the DENV serotypes and strains used that could explain the differences in cell tropism [40, 41], as has been reported for both pathogenic and non-pathogenic West Nile virus (WNV) strains [42]. Our study also shows that the neuron cell model employed was permissive to infection by DENV 1-4. This observation is in agreement with previous studies reporting a diverse *in vivo* viral tropism for neurons of the hippocampus, anterior horns, olfactory bulb, and cerebral cortex. In addition, apoptosis has been shown to occur in human and murine neurons both *in vivo* and *in vitro* as a result of DENV infection [43–47]. Furthermore, observations from autopsies showed extensive neuropathological alterations, including distinct neuronal abnormalities in which many neurons were acidophilic and exhibited visible cytoplasm shrinkage [48].

The invasion of host cells by viruses is first initiated by the attachment to the cell surface through cellular receptors; however, in the case of infection of the CNS by DENV, the identity of the viral receptor is still unclear. In the present study, we used lectins to explore putative receptors bearing carbohydrate residues or glycans that are potentially targeted by DENV during early infection of brain ECs. We observed that high-mannose glycans were not the primary receptors used to initiate infection of ECs especially for DENV1 and 4, where inhibition with the corresponding lectin was below 20%. Consistent with the findings of Martínez-Barragán and del Angel [49], we determined that DENV4 as well as serotypes 1 and 2 preferred terminal α-mannose for infection. These differences may be due to the different cells used in various studies. Regarding the role of GlcNAc residues, we found that all DENV serotypes except for serotype 1 utilized these residues in the infection of bEnd.3 cells. A study by Wichit et al. [50] demonstrated that β-GlcNAc residues may play a critical role in the binding of DENV to the host cell surface. The study characterized a neutral glycosphingolipid, nLc_4Cer, which has the carbohydrate moiety Galβ1-4GlcNAcβ1-3Galβ1-4Glcβ'Cer, which is present on LLC-MK2 cells. However, we could not determine whether our DENV strain targeted the same glycosphingolipid due to the limited number of lectins available to characterize the whole carbohydrate chain.

We further identified carbohydrate residues on the DENV E protein that might play a role in facilitating infection in our EC model. The E protein is the main virion surface component, which binds to receptors present on the surface of host cells, resulting in endocytosis of the virus particle. It

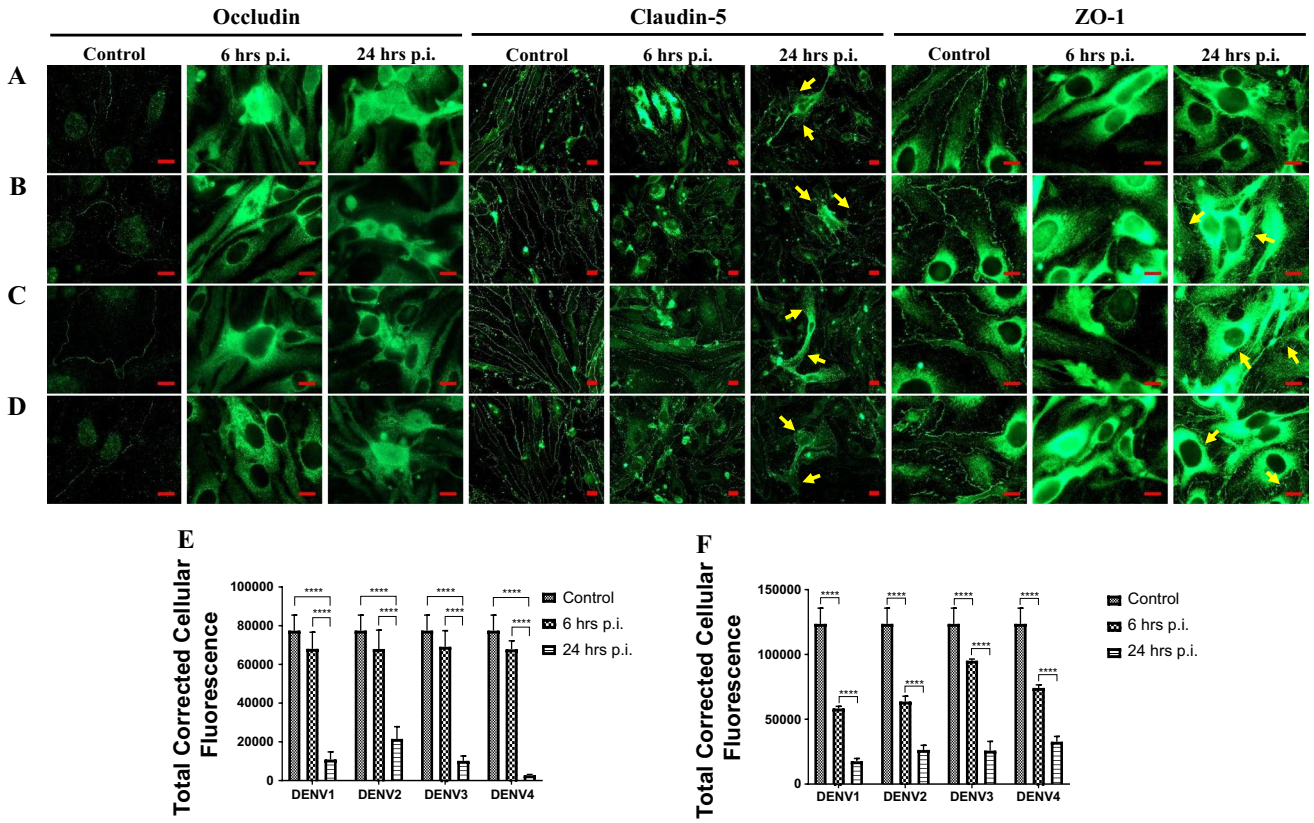

Fig. 6 Localization of tight-junction proteins and their degradation in DENV-infected bEnd.3 cells 6 hours and 24 hours postinfection (p.i.). A) DENV1, B) DENV2, C) DENV3 and D) DENV4. Peripheral fluorescence intensities of E) claudin-5 and F) ZO-1 were further analyzed using FIJI/ImageJ software. Total corrected cellular fluorescence (TCCF) was calculated by measuring the peripheral intensity and presented as the mean ± SD (n = 18-20). Asterisks indicate significance (****, $p < 0.0001$). Scale = 50 µm

is believed that carbohydrate chains found on the E protein play an important role in infection of the host cell at the early step of host receptor binding. The carbohydrates that are attached to the E protein have not been fully characterized, although the crystal structure of the glycoprotein has been determined [51]. In general, the presence of N-glycans on the E protein regulates proper protein folding, its interaction with receptors, and immunogenicity [52]. The E protein possesses two potential N-linked glycosylation sites at Asn67 and Asn153 [53], and the relevance of has sites have been studied extensively. Mondotte et al. [54] have shown that the absence, through mutation, of a carbohydrate at position 67 decreases the number of new infectious particles assembled but did not hinder viral entry or translation and replication of the genome. The sugars that are added to the E protein have been reported to be heterogeneous in structure and composition [55], and many studies have shown that DENV glycoproteins derived from mosquito cells have a combination of high-mannose and paucimannose glycans [52, 56].

The presence of high-mannose glycans on mosquito-derived DENV glycoproteins helps to enhance their interaction with DC-SIGN, which facilitates DENV entry into immature dendritic cells in the skin following a bite from an infected mosquito [52]. However, our results have shown that DENV, especially DENV1 and 2, did not depend on the presence of high-mannose-rich glycans for successful infection of brain ECs, but rather branching mannose glycans, as has been observed by Hung et al. [57], who showed that α-linked terminal mannose residues found in the E protein contribute to binding and penetration of C6/36 and baby hamster kidney fibroblast (BHK) cells. Our findings are also supported by the observation that a DENV isolate that was resistant to the lectin HHA (which is specific for α-mannose residues) due to the lack of both N-glycosylation sites on the E protein was not able to infect DC-SIGN^{+} dendritic cells but was able to establish a productive infection and replicate in DC-SIGN^{-} and carbohydrate-independent cells such as Huh7, BHK-21, Vero and C6/36 cells [52].

Studies have shown that the number and location of glycosylation motifs on the E protein vary significantly within dengue virus subtypes [56, 58]. Glycosylation motifs have been observed commonly in domain I at residues N153 or N154, but the addition of a glycan at these residues is not an absolute requirement for infectivity. Although glycosylation

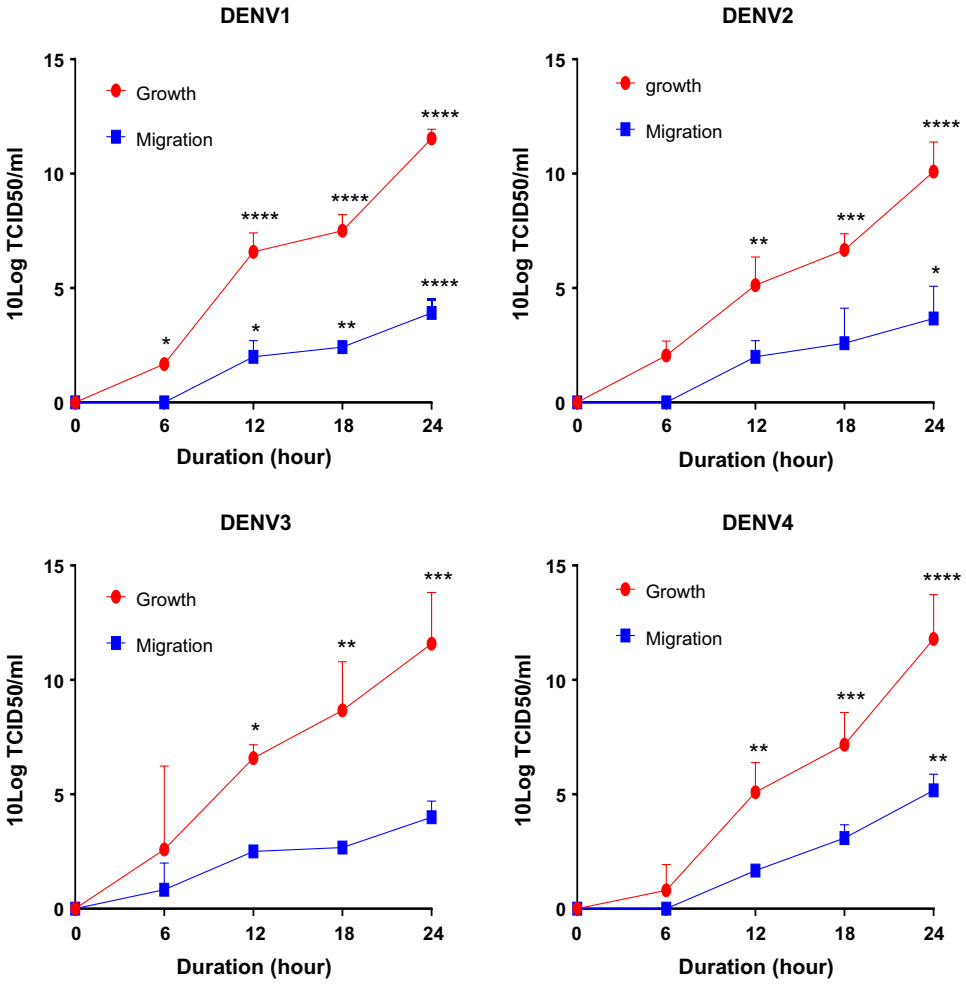

Fig. 7 Kinetics and migration of DENV across the BBB model. The cells were grown on Transwells (polyester insert, 0.4 µm pore size) and infected with the virus at an MOI of 5. At specific time points, viruses in the apical and basal compartment were harvested and titrated using a $TCID_{50}$ assay. Asterisks indicate significance (*, $p < 0.05$; **, $p < 0.01$; ***, $p < 0.001$; ****, $p < 0.0001$)

of this residue is not essential, several studies have shown that mutations affecting the N-linked glycosylation sites of the E glycoprotein may have an effect on virus-mediated membrane fusion and neurovirulence [59–61]. Differences in the amino acid sequence have been observed between the four wild-types DENV serotypes at amino acid 154, which is glutamic acid in both DENV1 [62] and DENV3 [63] and aspartic acid in both DENV2 [64] and DENV4 [65]. Hence, we can hypothesize that these differences may dictate the different requirement of glycan residues on E glycoprotein and for the infection of bEnd.3 cells. Another N-linked glycosylation motif of DENV is at N67, which mediates infection of dendritic cells bearing DC-SIGN receptors and is essential for viral assembly and exit [54, 66]. Removal of the N67 glycan has been shown to adversely affect viral fitness and to reduce cell infectivity [67].

To study the mechanism of BBB invasion by DENV, we used our established triple co-culture *in vitro* BBB model and infected it with our DENV isolates. We determined the ability of DENV to cross the BBB model and whether the crossing was accompanied by BBB destruction and increased permeability. Various studies have routinely used models that were composed of monolayers of brain microvascular ECs co-cultured with astrocytes for virus transmigration studies [38, 68–70]. Our results have shown the release of infectious virus in the lower compartment of the *in vitro* BBB model, which indicates the ability of cell-free DENV to migrate across the BBB. We detected very little to no DENV in the lower compartment at 6 hours after infection, but virus particles were detected at later time points. We observed that DENV crossed the membrane only after 12 hours postinfection in parallel to an increase in the paracellular influx of sucrose – a finding compatible with paracellular transport. In accordance with our data, it has been shown previously that DENV infection can induce cell apoptosis in human dermal microvascular endothelial cells (HMEC-1), suggesting that the virus might directly cause the breakdown of the BBB to enter the CNS [71]. A recent study has also shown that DENV was able to cross a BBB model composed of primary mouse brain ECs paracellularly by disrupting the integrity of this BBB in the process [38].

Paracellular transport of molecules or pathogens may occur following changes in cell morphology due to extensive modification of TJs and activation of ECs. In this

study, we assessed the movement of solutes across the model instead of measuring transendothelial electrical resistance (TEER). TEER measures the movement of ions through the barrier, and since ions cross the barrier not only via the paracellular pathway but also through transporters and ion pores, TEER is not directly indicative of a restrictive barrier of the cell layers [72]. We showed that the co-culture model under normal conditions exhibited low sucrose and albumin permeability, which indicated close connections mediated by TJ proteins. However, at 6 hours postinfection and at later time points, we observed a significant increase in sucrose permeability, which was suggestive of a disruption of the barrier linked to changes in TJ protein localization. Liu et al. [73] observed an increase in permeability of DENV-infected HUVECs only at later stages of infection, i.e., after prolonged infection, but not at earlier stages of infection.

Disruption and redistribution of TJ proteins has been suggested to be a part of the mechanism by which BBB permeability increases. To support this suggestion, we examined the expression of TJ proteins in DENV-infected brain ECs at the protein level using Western blot. In addition, we used an immunofluorescence assay to stain TJ proteins, specifically occludin, claudin-5, and ZO-1, to visualize the integrity of the barrier and determine the location of these proteins in uninfected and infected cells. We found that infection of ECs with DENV resulted in significant changes in the expression of claudin-5 and ZO-1 during peak virus production. We also observed that the infection significantly altered the peripheral distribution of the three TJ proteins investigated. DENV infection has been reported to cause the displacement of occludin from the periphery to the cytoplasm in infected HMEC-1 cells [74], as was observed in this study. Furthermore, Kanlaya et al. [75] observed a decrease in the expression of ZO-1 in a DENV-infected EC line.

Other studies have also demonstrated a decrease in the expression of claudin-5, along with ZO-1, occludins, and junctional adhesion molecules (JAMs), upon viral infections, resulting in the disruption of the BBB and an increase in the severity of the infection [76, 77]. In addition, HIV-1 and HIV-1 Tat protein have been reported to cause damage to the BBB through modification of claudin-5, thereby allowing HIV-1 to enter the brain [78]. A number of studies on the infection of human brain microvascular ECs by neurotropic viruses, including simian immunodeficiency virus (SIV) [79], human cytomegalovirus (HCMV) [80], and human T-lymphotropic virus 1 (HTLV-1) [81], have demonstrated that infection caused a decrease and/or redistribution of TJ proteins. Hence, the observation of the modulation and early redistribution of occludin, claudin-5 and ZO-1 may elucidate the mechanism of virus passage through the endothelial monolayer in a paracellular manner.

Conclusion

We report that all brain cell models used in this study were sensitive to DENV infection. bEnd.3 cells were also able to support the growth of DENV, producing high virus titers as infection progressed. We found that the carbohydrate moieties on the E glycoprotein required for brain EC infection and the role of these moieties were serotype-specific. Infection resulted in increased permeability of the BBB model as early as 6 hours postinfection, allowing DENV to cross the BBB model paracellularly. Our results also suggest that invasion was mediated by morphological changes in ECs and by the disruption as well as redistribution of TJ proteins, including occludin, claudin-5, and ZO-1. These alterations were responsible for compromising the integrity of the BBB and thus facilitating the paracellular movement of DENV across the BBB. However, other possible mechanisms of DENV entry into the brain also warrant further investigation.

Acknowledgements This work is supported by Universiti Brunei Darussalam. Idris F is a recipient of the Graduate Research Scholarships (GRS), Universiti Brunei Darussalam.

Funding This research did not receive any specific grant from funding agencies in the public, commercial, or not-for-profit sectors.

Compliance with ethical standards

Conflict of interest The authors declare that they have no conflict of interest.

Ethical approval This article does not contain any studies with human participants or animals performed by any of the authors.

References

1. Pardridge WM (1999) Blood-brain barrier biology and methodology. J Neurovirol 5:556–569
2. Abbott NJ, Patabendige AAK, Dolman DEM, Yusof SR, Begley DJ (2010) Structure and function of the blood-brain barrier. Neurobiol Dis 37:13–25
3. Spindler KR, Hsu TH (2012) Viral disruption of the blood-brain barrier. Trends Microbiol 20:282–290
4. Gralinski LE, Ashley SL, Dixon SD, Spindler KR (2009) Mouse adenovirus type 1-induced breakdown of the blood-brain barrier. J Virol 83:9398–9410
5. Erbar S, Maisner A (2010) Nipah virus infection and glycoprotein targeting in endothelial cells. Virol J 7:305
6. McMinn PC, Dalgarno L, Weir RC (1996) A comparison of the spread of Murray Valley encephalitis viruses of high or low neuroinvasiveness in the tissues of Swiss mice after peripheral inoculation. Virology 220:414–423
7. King NJ, Getts DR, Getts MT, Rana S, Shrestha B, Kesson AM (2007) Immunopathology of flavivirus infections. Immunol Cell Biol 85:33–42
8. Bai F, Kong KF, Dai J, Qian F, Zhang L, Brown CR, Fikrig E, Montgomery RR (2010) A paradoxical role for neutrophils in the pathogenesis of West Nile virus. J Infect Dis 202:1804–1812

9. Verma S, Lo Y, Chapagain M, Lum S, Kumar M, Gurjav U, Luo H, Nakatsuka A, Nerurkar VR (2009) West Nile virus infection modulates human brain microvascular endothelial cells tight junction proteins and cell adhesion molecules: transmigration across the in vitro blood-brain barrier. Virology 385:425–433
10. Misra UK, Kalita J (2010) Overview: Japanese encephalitis. Prog Neurobiol 91:108–120
11. Aleyas AG, George JA, Han YW, Rahman MM, Kim SJ, Han SB, Kim BS, Kim K, Eo SK (2009) Functional modulation of dendritic cells and macrophages by Japanese encephalitis virus through MyD88 adaptor molecule-dependent and -independent pathways. J Immunol 183:2462–2474
12. Cao S, Li Y, Ye J, Yang X, Chen L, Liu X, Chen H (2011) Japanese encephalitis virus wild strain infection suppresses dendritic cells maturation and function, and causes the expansion of regulatory T cells. Virol J 8:39
13. Chen ST, Liu RS, Wu MF, Lin YL, Chen SY, Tan DT, Chou TY, Tsai IS, Li L, Hsieh SL (2012) CLEC5A regulates Japanese encephalitis virus-induced neuroinflammation and lethality. PLoS Pathog 8:e1002655
14. Solomon T, Dung NM, Vaughn DW, Kneen R, Thao LT, Raengsakulrach B, Loan HT, Day NP, Farrar J, Myint KS, Warrell MJ, James WS, Nisalak A, White NJ (2000) Neurological manifestations of dengue infection. Lancet 255:1053–1059
15. Carod-Artal FJ, Wichmann O, Farrar J, Gascón J (2013) Neurological complications of dengue virus infection. Lancet Neurol 12:906–919
16. Dalrymple NA, Mackow ER (2012) Roles for endothelial cells in dengue virus infection. Adv Virol 2012:840654
17. Cardier JE, Mariño E, Romano E, Taylor P, Liprandi F, Bosch N, Rothman AL (2005) Proinflammatory factors present in sera from patients with acute dengue infection induce activation and apoptosis of human microvascular endothelial cells: possible role of TNF-alpha in endothelial cell damage in dengue. Cytokine 30:359–365
18. Lin CF, Wan SW, Chen MC, Lei HY, Lin YS (2007) Increased dengue virus-infected endothelial cell apoptosis caused by antibodies against nonstructural protein 1. Den Bull 31:111–117
19. Hapuarachchi HC, Chua RC, Shi Y, Thein TL, Lee LK, Lee KS, Lye DC, Ng LC, Leo YS (2015) Clinical outcome and genetic differences within a monophyletic Dengue virus type 2 population. PLoS One 10:e0121696
20. Chaturvedi UC, Dhawan R, Khanna M, Mathur A (1991) Breakdown of the blood-brain barrier during dengue virus infection of mice. J Gen Virol 72:859–866
21. Velandia-Romero ML, Acosta-Losada O, Castellanos JE (2012) In vivo infection by neuroinvasive neuro-virulent dengue virus. J Neurovirol 18:374–387
22. Zonta M, Angulo MC, Gobbo S, Rosengarten B, Hossmann KA, Pozzan T, Carmignoto G (2003) Neuron-to-astrocyte signaling is central to the dynamic control of brain microcirculation. Nat Neurosci 6:43–50
23. Takata F, Dohgu S, Yamauchi A, Matsumoto J, Machida T, Fujishita K, Shibata K, Shinozaki Y, Sato K, Kataoka Y, Koizumi S (2013) In vitro blood-brain barrier models using brain capillary endothelial cells isolated from neonatal and adult rats retain age-related barrier properties. PLoS One 8:e55166
24. Zhang Z, McGoron AJ, Crumpler ET, Li C (2011) Co-culture based blood-brain barrier in vitro model, a tissue engineering approach using immortalized cell lines for drug transport study. Appl Biochem Biotechnol 163:278–295
25. Hubatsch I, Ragnarsson EG, Artursson P (2007) Determination of drug permeability and prediction of drug absorption in Caco-2 monolayers. Nat Protoc 2:2111–2119
26. Rosas-Arellano A, Villalobos-González JB, Palma-Tirado L, Beltrán FA, Cárabez-Trejo A, Missirlis F, Castro MA (2016) A simple solution for antibody signal enhancement in immunofluorescence and triple immunogold assay. Histochem Cell Biol 146:421–430
27. McCloy RA, Rogers S, Caldon CE, Lorca T, Castro A, Burgess A (2014) Partial inhibition of Cdk1 in G2 phase overrides the SAC and decouples mitotic events. Cell Cycle 13:1400–1412
28. Alen MMF, De Burghgraeve T, Kaptein SJF, Balzarini J, Neyts J, Schols D (2011) Broad antiviral activity of carbohydrate-binding agents against the four serotypes of dengue virus in monocyte-derived dendritic cells. PloS One 6:e21658
29. Malenovska H (2013) Virus quantitation by transmission electron microscopy, $TCID_{50}$, and the role of timing virus harvesting: a case study of three animal viruses. J Virol Methods 191:136–140
30. Cummings BS, Wills LP, Schnellmann RG (2012) Measurement of cell death in mammalian cells. Curr Protoc Pharmacol 12(12):8
31. Noguiera RM, Schatzmayr HG, de Filippis AM, dos Santos FB, da Cunha RV, Coelho JO, de Souza LJ, Guimarães FR, de Araújo ES, De Simone TS, Baran M, Teixeira G Jr, Miagostovich MP (2005) Dengue virus type 3, Brazil, 2002. Emerg Infect Dis 11:1376–1381
32. Balsitis SJ, Coloma J, Castro G, Alava A, Flores D, McKerrow JH, Beatty PR, Harris E (2009) Tropism of dengue virus in mice and humans defined by viral non-structural protein 3-specific immunostaining. Am J Trop Med Hyg 80:416–424
33. De Araújo JM, Schatzmayr HG, de Pilippis AM, Dos Santos FB, Cardoso MA, Britto C, Coelho JM, Nogueira RM (2009) A retrospective survey of dengue virus infection in fatal cases from an epidemic in Brazil. J Virol Methods 155:34–38
34. Jessie K, Fong MY, Devi S, Lam SK, Wong KT (2004) Localization of dengue virus in naturally infected human tissues, by immunohistochemistry and in situ hybridization. J Infect Dis 189:1411–1418
35. Avirutnan P, Malasit P, Seliger B, Bhakdi S, Husmann M (1998) Dengue virus infection of human endothelial cells leads to chemokine production, complement activation, and apoptosis. J Immunol 161:6338–6346
36. Chen HC, Hofman FM, Kung JT, Lin YD, Wu-Hsieh BA (2007) Both virus and tumor necrosis factor alpha are critical for endothelium damage in a mouse model of dengue virus-induced haemorrhage. J Virol 81:5518–5526
37. Oliveira ER, Amorim JF, Paes MV, Azevedo AS, Goncalves AJ, Costa SM, Mantuano-Barradas M, Póvoa TF, de Meis J, Basílio-de-Oliveira CA, Nogueira AC, Alves AM (2016) Peripheral effects induced in BALB/c mice infected with DENV by the intracerebral route. Virology 489:95–107
38. Velandia-Romero ML, Calderón-Peláez MA, Castellanos JE (2016) In vitro infection with dengue virus induces changes in the structure and function of the mouse brain endothelium. PLoS One 11:e0157786
39. Imbert J, Guevera P, Ramos-Castañeda J, Ramos C, Sotelo J (1994) Dengue virus infects mouse cultured neurons but not astrocytes. J Med Virol 42:228–233
40. Elena SF (2002) Restrictions to RNA virus adaptation: an experimental approach. Antonie Van Leeuwenhoek 81:135–142
41. Whitehorn J, Simmons CP (2011) The pathogenesis of dengue. Vaccine 29:7221–7228
42. Hussmann KL, Fredericksen BL (2014) Differential induction of CCL5 by pathogenic and non-pathogenic strains of West Nile virus in brain endothelial cells and astrocytes. J Gen Virol 95:862–867
43. Desprès P, Plamand M, Ceccaldi PE, Deubel V (1996) Human isolates of dengue type 1 virus induce apoptosis in mouse neuroblastoma cells. J Virol 70:4090–4096
44. Jan JT, Chen BH, Ma SH, Liu CI, Tsai HP, Wu HC, Jiang SY, Yang KD, Shaio MF (2000) Potential dengue virus-triggered apoptotic pathway in human neuroblastoma cells: arachidonic

acid, superoxide anion, and NF-kappaB are sequentially involved. J Virol 74:8680–8691
45. An J, Zhou DS, Kawasaki K, Yasui K (2003) The pathogenesis of spinal cord involvement in dengue virus infection. Virchows Arch 442:472–481
46. Sánchez-Burgos G, Hernández-Pando R, Campbell IL, Ramos-Castañeda J, Ramos C (2004) Cytokine production in brain of mice experimentally infected with dengue virus. Neuroreport 15:37–42
47. Ho MR, Tsai TT, Chen CL, Jhan MK, Tsai CC, Lee YC, Chen CH, Lin CF (2017) Blockade of dengue virus infection and viral cytotoxicity in neuronal cells in vitro and in vivo by targeting endocytic pathways. Sci Rep 7:6910
48. Chimelli L, Hahn MD, Netto MB, Ramos RG, Dias M, Gray F (1990) Dengue: neuropathological findings in 5 fatal cases from Brazil. Clin Neuropathol 9:157–162
49. Martínez-Barragán JJ, del Angel RM (2001) Identification of a putative coreceptor on Vero cells that participates in dengue 4 virus infection. J Virol 75:7818–7827
50. Wichit S, Jittmittraphap A, Hidari KI, Thaisomboonsuk B, Petmitr S, Ubol S, Aoki C, Itonori S, Morita K, Suzuki T, Suzuki Y, Jampangern W (2011) Dengue virus type 2 recognizes the carbohydrate moiety of neutral glycosphingolipids in mammalian and mosquito cells. Microbiol Immuno. 55:135–140
51. Hidari KI, Suzuki T (2011) Antiviral agents targeting glycans on dengue virus E-glycoprotein. Expert Rev Anti Infect Ther 9:983–985
52. Alen MM, Dallmeier K, Balzarini J, Neyts J, Schols D (2012) Crucial role of the N-glycans on the viral E-envelope glycoprotein in DC-SIGN mediated dengue virus infection. Antiviral Res 96:280–287
53. Hacker K, White L, de Silva AM (2009) N-linked glycans on dengue viruses grown in mammalian and insect cells. J Gen Virol 90:2097–2106
54. Mondotte JA, Lozach PY, Amara A, Gamarnik AV (2007) Essential role of dengue virus envelope protein N glycosylation at asparagine-67 during viral propagation. J Virol 81:7136–7148
55. Smith GW, Wright PJ (1985) Synthesis of proteins and glycoproteins in dengue type 2 virus-infected vero and Aedes albopictus cells. J Gen Virol 66:559–571
56. Johnson AJ, Guirakhoo F, Roehrig JT (1994) The envelope glycoproteins of dengue 1 and dengue 2 viruses grown in mosquito cells differ in their utilization of potential glycosylation sites. Virology 203:241–249
57. Hung SL, Lee PL, Chen LK, Kao CL, King CC (1999) Analysis of the steps involved in Dengue virus entry into host cells. Virology 257:156–167
58. Ishak H, Takegami T, Kamimura K, Funada H (2001) Comparative sequences of two type 1 dengue virus strains possessing different growth characteristics in vitro. Microbiol Immunol 45:327–331
59. Guirakhoo F, Hunt AR, Lewis JG, Roehrig JT (1993) Selection and partial characterization of dengue 2 virus mutants that induce fusion at elevated pH. Virology 194:219–223
60. Kawano H, Rostapshov V, Rosen L, Lai CJ (1993) Genetic determinants of dengue type 4 virus neurovirulence for mice. J Virol 67:6567–6575
61. Sanchez IJ, Ruiz BH (1996) A single nucleotide change in the E protein gene of dengue virus 2 Mexican strain affects neurovirulence in mice. J Gen Virol 77:2541–2545
62. Chu MC, O'Rourke EJ, Trent DW (1989) Genetic relatedness among structural protein genes of dengue 1 virus strains. J Gen Virol 70:1701–1712
63. Osatomi K, Sumiyoshi H (1990) Complete nucleotide sequence of dengue type 3 virus genome RNA. Virology 176:643–647
64. Deubel V, Kinney RM, Trent DW (1988) Nucleotide sequence and deduced amino-acid sequence of the nonstructural proteins of dengue type 2 virus, Jamaica genotype: comparative analysis of the full-length genome. Virology 165:234–244
65. Zhao B, Mackow E, Buckler-White A, Markoff L, Chanock RM, Lai CJ, Makino Y (1986) Cloning full length dengue type 4 viral DNA sequences: analysis of genes coding for structural proteins. Virology 156:77–88
66. Pokidysheva E, Zhang Y, Battisti AJ, Bator-Kelly CM, Chipman PR, Xiao C, Gregorio GG, Hendrickson WA, Kuhn RJ, Rossmann MG (2006) Cryo-EM reconstruction of dengue virus in complex with the carbohydrate recognition domain of DC-SIGN. Cell 124:485–493
67. Bryant JE, Calvert AE, Mesesan K, Crabtree MB, Volpe KE, Silengo S, Kinney RM, Huang CYH, Miller BR, Roehrig JT (2007) Glycosylation of the dengue 2 virus E protein ay N67 is critical for the virus growth in vitro but not for growth in intrathoracically inoculated *Aedes aegypti* mosquitoes. Virology 366:415–423
68. Kanmogne GD, Schall K, Leibhart J, Knipe B, Gendelman HE, Persidsky Y (2007) HIV-1 gp120 compromises blood-brain barrier integrity and enhances monocyte migration across blood-brain barrier: implication for viral neuropathogenesis. J Cereb Blood Flow Metab 27:123–134
69. Chaudhuri A, Yang B, Gendelman HE, Persidsky Y, Kanmogne GD (2008) STAT1 signaling modulates HIV-1-induced inflammatory responses and leukocyte transmigration across the blood-brain barrier. Blood 111:2062–2072
70. Mahajan SD, Aalinkeei R, Sykes DE, Reynolds JL, Bindukumar B, Adal A, Qi M, Toh J, Xu G, Prasad PN, Schwartz SA (2008) Methamphetamine alters blood brain barrier permeability via the modulation of tight junction expression: implication for HIV-1 neuropathogenesis in the context of drug abuse. Brain Res 1203:133–148
71. Vásquez Ochoa M, García Cordero J, Gutiérrez Castañeda B, Santos Argumedo L, Villegas Sepúlveda N, Cedillo Barrón L (2009) A clinical isolate of dengue virus and its proteins induce apoptosis in HMEC-1 cells: a possible implication in pathogenesis. Arch Virol 154:919–928
72. Hellinger E, Veszelka S, Tóth AE, Walter F, Kittel A, Bakk ML, Tihanyi K, Háda V, Nakagawa S, Duy TD, Niwa M, Deli MA, Vastag M (2012) Comparison of brain capillary endothelial cell-based and epithelial (MDCK-MDR1, Caco-2, and VB-Caco-2) cell-based surrogate blood-brain barrier penetration models. Eur J Pharm Biopharm 82:340–351
73. Liu P, Woda M, Ennis FA, Libraty DH (2009) Dengue virus infection differentially regulates endothelial barrier function over time through type I interferon effects. J Infect Dis 200:191–201
74. Talavera D, Castillo AM, Dominguez MC, Gutierrez AE, Meza I (2004) IL8 release, tight junction and cytoskeleton dynamic reorganization conducive to permeability increase are induced by dengue virus infection of microvascular endothelial monolayers. J Gen Virol 85:1801–1813
75. Kanlaya R, Pattanakitsakul SN, Sinchaikul S, Chen ST, Thongboonherd V (2009) Alterations in actin cytoskeletal assembly and junctional protein complexes in human endothelial cells induced by dengue virus infection and mimicry of leukocyte transendothelial migration. J Proteome Res 8:2551–2562
76. Dallasta LM, Pisarov LA, Esplen JE, Werley JV, Moses AV, Nelson JA, Achim CL (1999) Blood-brain barrier tight junction disruption in human immunodeficiency virus-1 encephalitis. Am J Pathol 155:1915–1927
77. Diamond MS, Klein RS (2004) West Nile Virus: crossing the blood-brain barrier. Nat Med 10:1294–1295

78. András IE, Toborek M (2011) HIV-1-induced alterations of claudin-5 expression at the blood-brain barrier level. Methods Mol Biol 762:355–370
79. Luabeya MK, Dallasta LM, Achim CL, Pauza CD, Hamilton RL (2000) Blood-brain barrier disruption in simian immunodeficiency virus encephalitis. Neuropathol Appl Neurobiol 26:454–462
80. Bentz GL, Jarguin-Pardo M, Chan G, Smith MS, Sinzger C, Yurochko AD (2006) Human cytomegalovirus (HCMV) infection of endothelial cells promotes naïve monocyte extravasation and transfer of productive virus to enhance hematogenous dissemination of HCMV. J Virol 80:11539–11555
81. Afonso PV, Ozden S, Prevost MC, Schmitt C, Seilhean D, Weksler B, Couraud PO, Gessain A, Romero IA, Ceccaldi PE (2007) Human blood-brain barrier disruption by retroviral-infected lymphocytes: role of myosin light chain kinase in endothelial tight-junction disorganization. J Immunol 179:2576–2583